ACS APPLIED MATERIALS & INTERFACES

Research Article

www.acsami.org

Supercapacitor Electrodes Based on Layered Tungsten Disulfide-Reduced Graphene Oxide Hybrids Synthesized by a Facile Hydrothermal Method

Satyajit Ratha and Chandra Sekhar Rout*

School of Basic Sciences, Indian Institute of Technology Bhubaneswar, Bhubaneswar 751013, India

Supporting Information

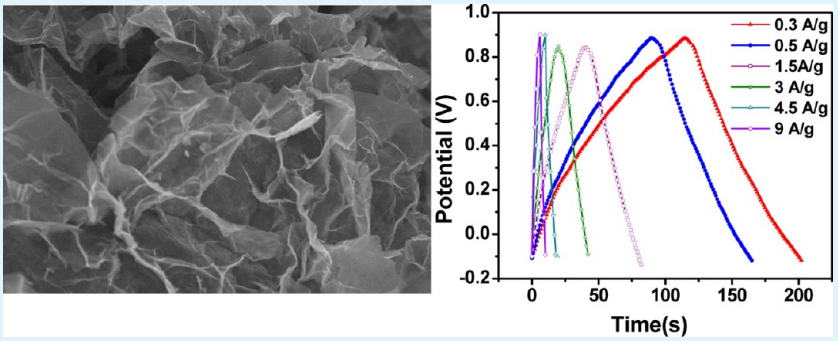

ABSTRACT: We report here the synthesis of layer structured WS_2/reduced graphene oxide (RGO) hybrids by a facile hydrothermal method for its possible application as supercapacitor materials in energy storage devices. The prepared two-dimensional materials are characterized thoroughly by various analytical techniques to ascertain their structure and to confirm the absence of any impurities. Two-electrode capacitance measurements have been carried out in aqueous 1 M Na_2SO_4. The WS_2/RGO hybrids exhibited enhanced supercapacitor performance with specific capacitance of 350 F/g at a scan rate of 2 mV/s. The obtained capacitance values of WS_2/RGO hybrids are about 5 and 2.5 times higher than bare WS_2 and RGO sheets. Because of the unique microstructure with combination of two layered materials, WS_2/RGO hybrids emerge as a promising supercapacitor electrode material with high specific capacitance, energy density, and excellent cycling stability.

KEYWORDS: *layered materials, metal chalcogenides, WS_2, graphene oxide, supercapacitors*

1. INTRODUCTION

Following the graphene[1,2] revolution, graphene analogues of other inorganic layered materials with graphene-like structure, especially those with ultrathin nanosheets of transition metal chalcogenides (TMD) with single or few atomic layers, have received significant attention from the scientific community because of their interesting and useful properties as well as their direct applications in various nanoelectronic and energy storage devices.[3−5] Among the TMD layered compounds, MoS_2,[3−5] $MoSe_2$,[6−8] WS_2,[3−5] and WSe_2[9] are semiconductors; VS_2[10] and VSe_2[11] are metallic; HfS_2[12] is an insulator; and NbS_2,[13] $NbSe_2$,[14] $NbTe_2$,[15] and $TaSe_2$[16,17] are superconductors. Therefore, developing a TMD and its hybrid materials by a cost-effective, simple method for energy storage and energy conversion devices is extremely urgent.

Supercapacitors, also known as electrochemical capacitors are an important power source, which have been considered as one of the most promising energy-storage devices because of their many advantages, including high power density, faster charge/discharge processes, very long cycle life and relatively low cost.[18−22] Recently, two-dimensional (2D) layered materials including graphene,[18,19] reduced graphene oxide,[22−25] metal oxides,[26−31] metal chalcogenides,[32−38] and their composites[39] have shown to be efficient and promising materials for high performance supercapacitor electrodes due to their high surface area and large in-plane conductivity. Metal sulfides are known to be electrochemically active materials for supercapacitor applications, but to date very few metal sulfides have been employed to fabricate supercapacitor electrodes.[32−37] Because of their synergic advantages of high conductivity and high surface area, VS_2 nanosheets have been employed to fabricate in plane supercapacitor electrodes.[32] Ajayan and co-workers reported fabrication of micro-supercapacitors based on 2D MoS_2 films prepared by a low-cost spray painting technique and subsequent laser patterning.[33] Supercapacitor electrodes based on CoS_2 and CoS_2/graphene hybrids have been shown as promising materials for energy storage.[34,35] Similarly, NiS sheets have been demonstrated as an electrode material for supercapacitor because of their large surface area and enhanced structural stability.[37,38] Hence, the success of applying a

Received: August 29, 2013
Accepted: October 14, 2013
Published: October 14, 2013

homogeneous or heterogeneous nanostructured materials for supercapacitor applications strongly depends on the following factors in particular: employment of proper synthesis methods to prepare the desired nanostructure; selection of a proper combination of different materials; designation and optimization of the heterogeneous nanostructure.[3−5]

WS_2 is a naturally occurring metal sulfide with intriguing electronic,[40,41] electrochemical[42−45] and electrocatalytic properties,[46,47] formed by 2D covalently bonded S−W−S layers separated by a van der Waals gap. Weak van der Waals interactions also hold the adjacent sulphur sheets together with a layer sequence S−W−S.[40,41] WS_2 possesses hexagonal crystal structure with space group *P*63/*mmc* and each WS_2 monolayer contains an individual layer of W atoms with 6-fold coordination symmetry, which are then hexagonally packed between two trigonal atomic layers of S atoms.[5,47] The WS_2 material has attracted attention for diverse applications in future nanoelectronic devices because of its 2D layered structure and direct-band gap.[41,42,47] But, supercapacitor electrodes based on WS_2 and its graphene hybrids have not been reported yet. W atoms possess a wide range of oxidation states varying from +2 to +6, suggesting WS_2 to be a promising typical pseudocapacitive material for energy storage applications. Here we report supercapacitor electrodes based on 2D WS_2 sheets and a composite material consisting of two layered materials WS_2 and RGO prepared by a simple hydrothermal method. The as-prepared nanocomposite exhibited enhanced and stable supercapacitive behaviour in two electrode capacitance measurements.

2. METHODS

Preparation of GO Solution and RGO. Graphene oxide (GO) synthesis was performed by a modified Hummers method reported elsewhere.[48] RGO was obtained by hydrothermal reaction of GO solution at 265 °C for 24 h.[48]

Preparation of Few Layered WS_2 Sheets. WS_2 sheets were synthesized by a one-step hydrothermal reaction. In a typical experiment, 3 mM WCl_6 (Sigma-aldrich, 99.98%) and 15 mM thioacetamide (C_2H_5NS, Sigma-Aldrich, ≥99%) were dissolved in 40 mL DI water and stirred for 1 h at room temperature by using a magnetic stirrer. The solution was transferred to a 50 mL stainless steel autoclave, heated up to 265 °C and kept for 24 h. After cooling naturally, the product was filtered, washed with DI water, and dried in a vacuum at 60 °C for 6 h.

Preparation of WS_2/RGO Hybrids. The WS_2/RGO hybrids was synthesized by the same hydrothermal reaction condition as that for WS_2 sheets. Eight milliliters of 5 mg/mL GO solution was added to the mixture of WCl_6 and thioacetamide and the total volume of the solution was maintained at 40 mL. The same processes mentioned for WS_2 sheets were followed. During the hydrothermal process, smaller size WS_2 sheets were coated on GO and subsequently GO transformed to RGO (Figure 1). Carbon content in the final product was 3 wt %, which was confirmed by elemental analysis.

Characterizations. The samples were characterized with X-ray diffraction (Rigaku, Minislex model) equipped with the following: Ni filtered Cu Kα radiation (40 kV, 100 mA, λ = 0.15418 nm), scanning electron microscopy (FEI ESEM QUANTA 200 3D) and high resolution transmission electron microscopy (FEI TECNAI TF-30) (HRTEM). The samples were also characterized by a Micro Raman spectrometer (Renishaw inVia Raman microscope) with a laser excitation wavelength of 532 nm and laser power of 1 mW/cm^2.

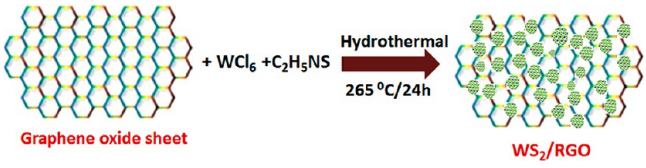

Figure 1. Schematic showing the hydrothermal synthesis process of WS_2/RGO hybrids.

Supercapacitor Fabrication and Measurements. Supercapacitors were fabricated using a swage-lok type two electrode cell. First the samples were dispersed in ethanol and ground for 1 h, followed by ultrasonication in a ice bath for 10 min to obtain a homogenous mixture. The mixture was then drop-casted on to the stain-less steel swage-lok type electrodes to achieve a mass of 2 mg on both the electrodes. The symmetric electrodes were separated by a porous cellulose nitrate membrane (Himedia, pore size 0.22 μm) soaked with 1 M aqueous Na_2SO_4 solution. Cycling voltammetry, charge-discharge and long cycling measurements in the two electrode configuration were performed by PG262A potentiostat/galvanostat (Technoscience Ltd., Bangalore, India) with working potential window between −0.1 and 0.9 V. Before taking the electrochemical data, the fabricated supercapacitor cells were activated by performing charge-discharge measurements for 1000 cycles.

To know about the pseudocapacitive behavior, we have performed cyclic voltammetry experiments in a three-electrode electrochemical cell with the samples loaded on glassy carbon as the working electrode, Ag/AgCl as the reference electrode, and platinum wire as the counter electrode. Glassy carbon electrodes (GCE) of 3.0 mm in diameter were polished with finer emery paper and 0.3 μm Al_2O_3 powder. The working electrodes were cleaned in an ultrasonic bath and dried in a vacuum. In a typical process for the sample loading, the WS_2/RGO was dispersed in ethanol to get a homogenous solution and drop coated on GCE and dried in vacuum followed by drop coating of 10 μL of Nafion solution and vacuum drying. Mass of the samples used was measured using a microbalance. Electrochemical experiments at slow scan rates were carried out in 1 M aqueous Na_2SO_4 solution as the electrolyte and the potential window for cycling was confined between −0.1 and 0.9 V.

Calculation of Capacitance. Cyclic voltammetry was performed at various scan rates (2 to 500 mV/s) for both three and two electrodes supercapacitors. Specific capacitance for the supercapacitors was calculated from the cyclic voltammogram measurements according to eq 1

$$C_{sp} = 2[ms(V_a - V_b)]^{-1} \int I(V)\mathrm{d}V \quad (1)$$

where $\int I\mathrm{d}V$ is the area under the curve, m is the mass of electrode used, s is the scan rate, and $(V_a - V_b)$ is the working window.

Galvanostatic charge−discharge measurements were performed for the supercapacitors to give a more accurate capacitance values. The specific capacitance was calculated from the constant current discharge curves, according to eqs 2, where I is the discharge current and $\mathrm{d}V/\mathrm{d}t$ is the slope of discharge curve.

$$C_{sp} = 2It/[m(V_a - V_b)\mathrm{slope}] \quad (2)$$

3. RESULTS AND DISCUSSION

FESEM images reveal that the thickness of stacked WS_2 sheets is ∼1−5 nm and their length is in the range of ∼1−3 μm (Figure 2). XRD analysis of the WS_2 sheets shows high crystalline hexagonal structure (Powder Diffraction File (PDF) No. 84-1398) without any other impurities. The XRD data of WS_2 sheets shows the direction of sheet growth is along the (002) direction (Figure 2c). Raman spectroscopy reveals the characteristic peaks of WS_2 in the 200−500 cm^{-1} range (Figure 2d). Transmission Elecron micrscopy (TEM) analysis demonstrates the formation of single crystalline, few-layered WS_2 sheets (Figure 3). The high-resolution transmission elecron microscopy (HRTEM) image revealed stacking of WS_2 (002) layers with an interplanar spacing of 0.62 nm and periodic

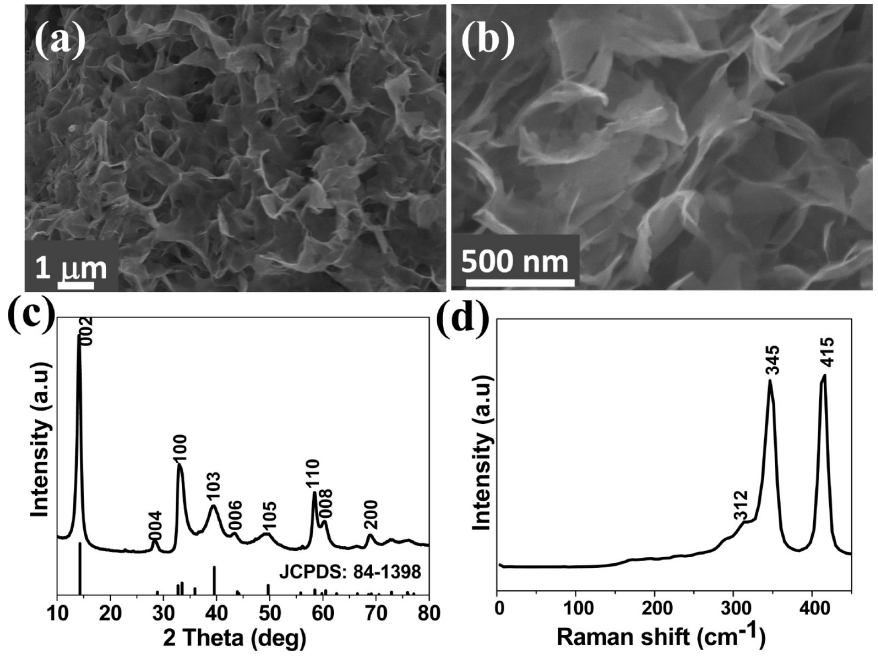

Figure 2. (a) Low- and (b) high-magnification FESEM images of WS_2 sheets. (c) XRD pattern and (d) Raman spectra of WS_2 sheets.

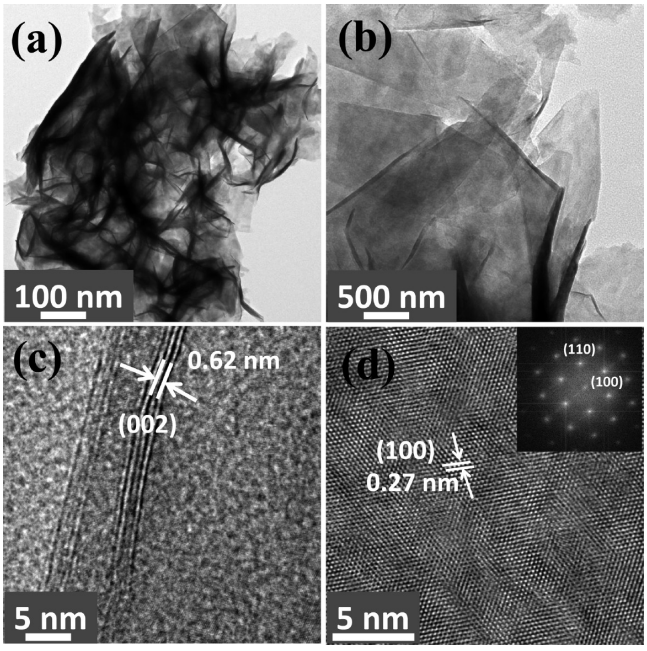

Figure 3. TEM analysis of WS_2 sheets: (a) low-and (b) high-magnification TEM images, (c) HRTEM image showing the layer spacing, (d) HRTEM image with inset showing electron diffraction pattern.

arrays of (100) planes with a spacing of 0.27 nm (Figure 3d). In the planar orientation, lattice fringes along (100) and (110) planes of the hexagonal WS_2 are clearly observed.

Because GO sheets exhibit enormously active edges and functional groups on their basal plane, they act as a novel substrate for the nucleation and subsequent growth of WS_2. Hence during hydrothermal reaction in GO solution, the tungsten precursor is reduced to form WS_2 on GO and GO transformed to RGO. Similarly, in the absence of GO sheets, WS_2 sheets are formed in the same hydrothermal method. Panels a and b in Figure 4 show the morphology and microstructure of the WS_2/RGO sheets. It is revealed that WS_2 sheets are coated on the RGO sheets and it exhibit a large number of protruding edges on the surface. XRD pattern of the WS_2/RGO composite shows a broad (002) peak and a more intense (100) peak as compared to the WS_2 sheets (Figure 4c). The broadness of the (002) peak indicates both smaller size and fewer layers for the WS_2 sheets. Also, it confirms the growth of a large number of protrusion edges along the (100) direction on RGO. Raman spectroscopy reveals presence of the characteristic peaks of WS_2 and the D (1348 cm^{-1}) and G (1587 cm^{-1}) bands of RGO in the WS_2/RGO hybrids (Figure 4d). In both the WS_2 sheets and the WS_2/RGO hybrids three bands are observed at 312, 345, and 415 cm^{-1}, which corresponds to the E_{1g}, $E_{2g}{}^1$, and A_{1g} modes, respectively.[49,50] The relative intensity ratio of the $E_{2g}{}^1$ and A_{1g} bands of WS_2 and WS_2/RGO are 0.98 and 1.07 respectively, which indicates that most of the WS_2 sheets consists of two stacked layers.[49] Recently, Berkdemir et al. revealed that ratio of $E_{2g}{}^1$ and A_{1g} bands vary between 2.2 and 0.8 for 1−3 layered WS_2, whereas it becomes 0.6 for bulk WS_2 samples.[49]

TEM images of WS_2-RGO sheets (Figure 5) indicate uniform coverage of WS_2 on RGO. HRTEM analysis reveals coating of thin layered, hexagonal WS_2 on RGO. X-ray photoelectron spectroscopy (XPS) analysis confirmed the formation of pure WS_2 phase in both WS_2 sheets and WS_2/RGO. Figure 6 shows W 4f, S 2p, and C 1s XPS spectra of WS_2/RGO hybrids and similar spectra are obtained for the WS_2 sheets. The peaks observed at 34.44 and 32.24 eV are attributed to $W4f_{5/2}$ and $W4f_{7/2}$, which are characteristic of the W^{4+} oxidation state.[40] The majority of the tungsten disulfide are present in the pristine form and the presence of the W−O peak at 37.2 eV suggests presence of very low content of surface oxide. The S 2p core level analysis demonstrates the existence of the S^{2-} species in the WS_2 and WS_2/RGO sheets, and the peaks at 161.8 and 163 eV can be indexed to S $2p_{3/2}$ and S $2p_{1/2}$, respectively.[44,48] The C 1s peak centered at 284.4 eV is ascribed to the presence of nonoxygenated sp^2 C in the basal plane of RGO, and the fitted peak observed at the higher

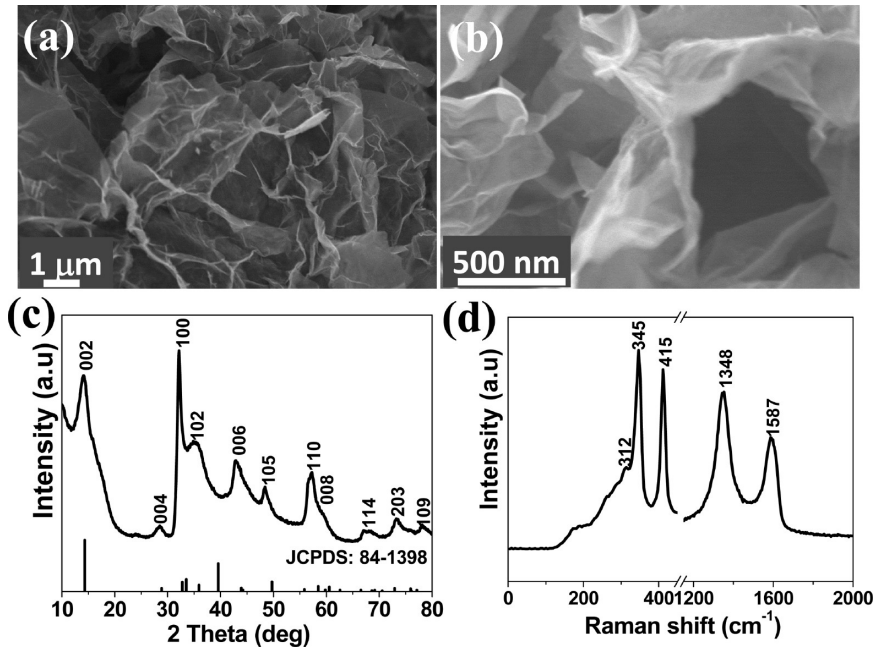

Figure 4. (a) Low- and (b) high-magnification FESEM images of WS_2/RGO hybrids. (c) XRD pattern and (d) Raman spectra of WS_2/RGO hybrids.

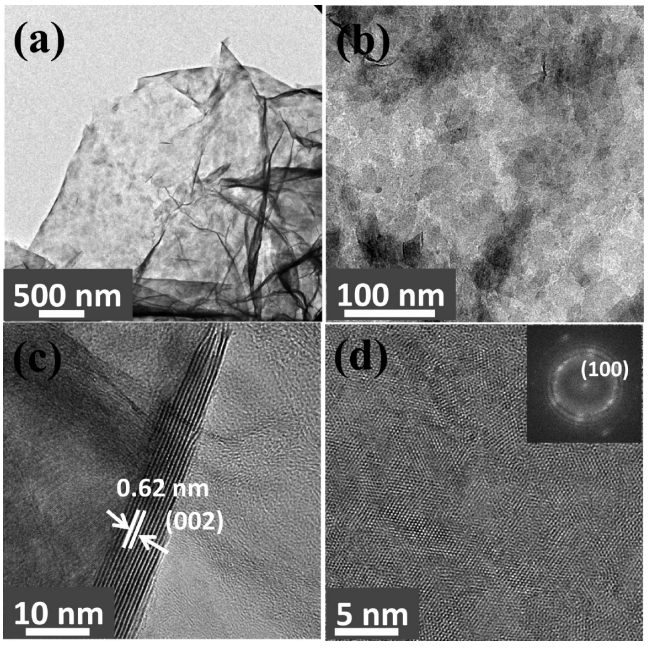

Figure 5. TEM analysis of WS_2/RGO hybrids: (a, b) low magnification TEM images, (c) HRTEM image showing the layer spacing, (d) HRTEM image with inset showing electron diffraction pattern.

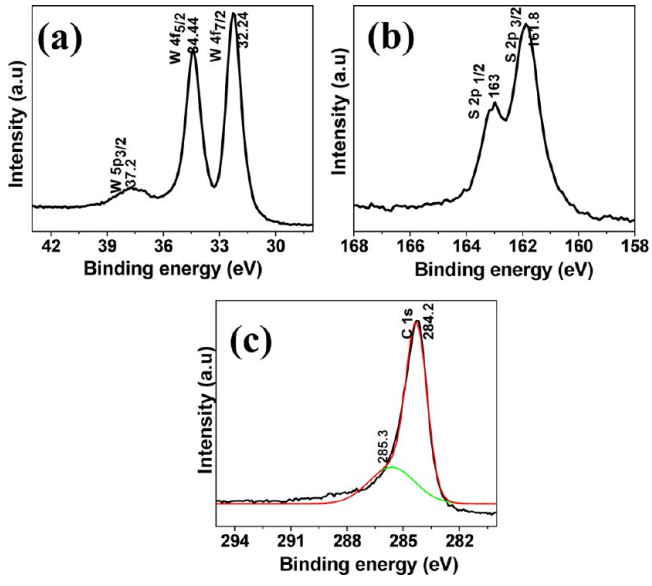

Figure 6. XPS spectra showing the (a) W 7f, (b) S 2p, and (c) C 1s core levels of the WS_2/RGO hybrids.

binding energy indicates the presence of a trace amount of oxygen-containing functional groups.[48]

Because of the unique microstructure with combination of two 2D materials and having high surface area due to their novel crystal structure, WS_2/RGO has a potential to significantly enhance the electrochemical performance as supercapacitor electrode. Enhanced supercapacitor performance should be attributed to the intercalation of Na^+ ions into the van der Waals gap of the WS_2 layers. In the WS_2/RGO hybrids, the large surface area and the nanoscale size of WS_2 and RGO greatly reduce the diffusion length over which both ions and electrons must transfer during the charge−discharge process. RGO helps to enhance the conductivity of the hybrids because there is uniform coverage of WS_2 on RGO and it facilitates fast transportation of electrons throughout the hybrid electrode material. *I*−*V* characteristics of WS_2 and WS_2/RGO films confirm the enhancement in conductivity of the WS_2/RGO hybrids as compared to only WS_2 sheets (see Figure S1 in the Supporting Information). We have investigated the electrochemical properties of the WS_2/RGO hybrids, WS_2 sheets and RGO by two electrode swage-lok cells in 1 M Na_2SO_4 electrolyte by using cyclic voltammetry (CV) and charge-discharge cycling. Figure 7a shows typical CV curves of the WS_2/RGO electrode at different scan rates. The CVs show

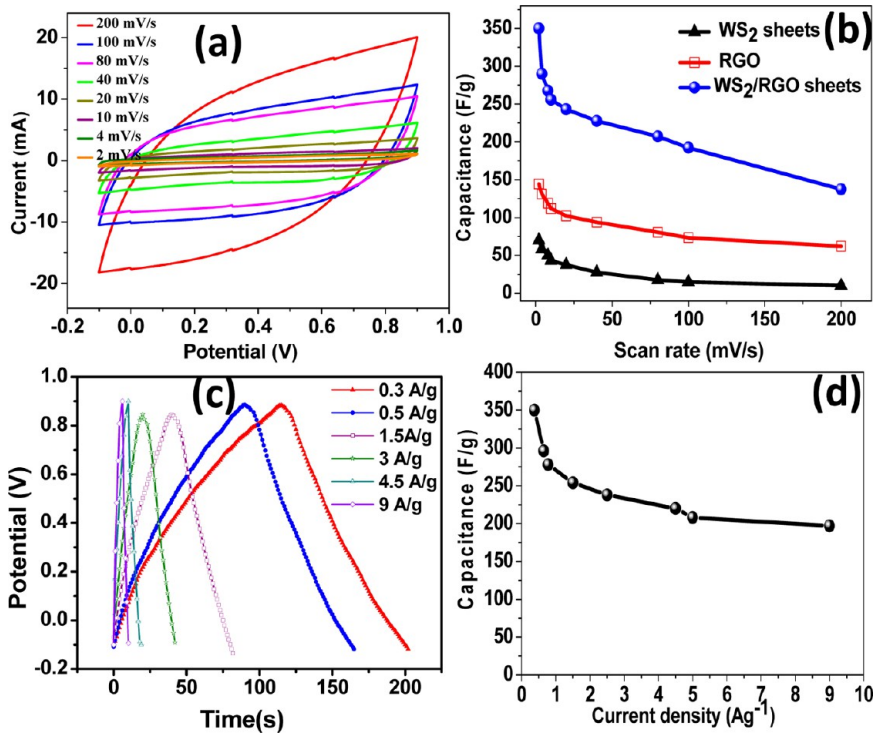

Figure 7. (a) Cyclic voltammograms at different scan rates of WS_2/RGO, (b) variation of specific capacitance with scan rate for WS_2/RGO, WS_2 and RGO. (c) Charge–discharge curves and (d) specific capacitance at different discharge current for WS_2/RGO hybrids.

nearly rectangular shapes at different scan rates indicating their potential as supercapacitors. Similarly, we have performed the cyclic voltammetry for WS_2 and RGO, which are shown in Figures S2a and S3a in the Supporting Information. Figure 7b shows the comparison of specific capacitance values obtained for the WS_2/RGO, WS_2, and RGO, respectively. A highest capacitance of 350 F/g is obtained for WS_2/RGO hybrids at a scan rate of 2 mV/s, whereas RGO and WS_2 sheets show a capacitance of 130 and 70 F/g. Hence, the capacitance value of WS_2/RGO hybrids at a scan rate of 2 mV/s is about 5 and 2.6 times higher than WS_2 and RGO sheets. Charge–discharge curves are obtained for WS_2/RGO, WS_2, and RGO at different discharge current. These curves are symmetric, indicating that the hybrid composite has a good electrochemical capacitive characteristic and superior reversible redox reaction. The specific capacitance are calculated from the galvanostatic charge/discharge curves at different discharge current according to eq 2. The highest specific capacitance of the WS_2/RGO hybrids is ~350 F/g for a discharge current density of 0.5 A g^{-1} (Figure 7d), which is in good agreement with the capacitance value obtained from the CVs. We have observed a decrease in capacitance at higher current density and scan rates that is due to the lower diffusion of charged ions at higher scan rates. Similar phenomena have been observed in literature for supercapacitors based on carbon based hybrid materials.[51,52] The supercapacitor performance of the WS_2/RGO hybrids is remarkably compared with the previous literature report on CoS_2/RGO composite, which exhibited a specific capacitance of 314 F/g.[37] The excellent capacitive performance of the WS_2/RGO hybrids is attributed to high electrical conductivity of the composite and homogenous coverage of thin layered WS_2 sheets on RGO sheets, facilitating the rapid transport of the electrolyte ions and increasing the electrochemical utilization of WS_2. The CV of WS_2/RGO at 2 mV/s shows hump peaks (see the Supporting Information, Figure S4), which is due to possible redox reaction ($WS_2 + Na^+ + e^- = WS\text{-}Na^+$) and similar types of reactions are proposed for MoS_2 and WS_2 based supercapacitors.[33,53,54] This makes faradaic contribution to the overall performance.

Long cycling life is another important requirement for supercapacitors. In this context, the cycling life test for the WS_2/RGO hybrids are carried out by performing the charge–discharge experiments over 1000 cycles at the current density of 3 Ag^{-1} (Figure 8). Interestingly, the specific capacitance of

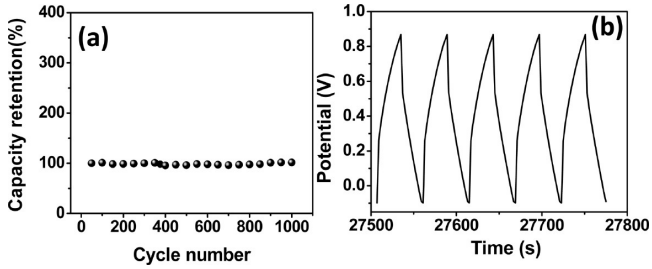

Figure 8. (a) Cycling stability performance of the WS_2/RGO supercapacitor electrodes at 3 A g^{-1}. (b) Last five charge–discharge cycles.

WS_2/RGO hybrids stays stable even after 1000 cycles. The electrochemical stability of the electrodes is also evidenced in the last five cycles of the discharge curves (Figure 8b), which shows that even after long period of charge-discharge, the curves remain undistorted and essentially symmetric. For the WS_2/RGO hybrids, the highest energy density is ~49 Wh/kg, whereas it is ~10 and ~20 Wh/kg for WS_2 and RGO sheets respectively (see Figure S5 in the Supporting Information). Hence WS_2/RGO hybrids emerge as one of the promising

supercapacitor electrode material because of their high specific capacitance, energy density, and excellent cycling stability.

4. SUMMARY

In summary, this work reports a simple synthesis method of preparing WS_2/RGO hybrids to achieve high performance supercapacitor electrodes. We have investigated the electrochemical supercapacitor properties of the WS_2/RGO hybrids, WS_2 sheets, and RGO by two-electrode measurements in 1 M Na_2SO_4 electrolyte by using cyclic voltammetry and charge−discharge cycling. WS_2/RGO hybrids showed significantly enhanced specific capacitance of 350 F/g at a scan rate of 2 mV/s, whereas RGO and WS_2 sheets showed a capacitance of 130 and 70 F/g. The WS_2/RGO hybrids also demonstrated excellent cycling stability and enhanced energy density of ∼49 Wh/kg. The excellent capacitive performance of the WS_2/RGO hybrids is attributed to high electrical conductivity of the composite and homogenous coverage of thin layered WS_2 sheets on RGO sheets, facilitating the rapid transport of the electrolyte ions and increasing the electrochemical utilization of WS_2. The enhanced electrochemical properties of the WS_2/RGO hybrids may lead to potential applications for high-performance supercapacitors.

■ ASSOCIATED CONTENT

Ⓢ Supporting Information

I−*V* characteristics, cyclic voltammograms, specific capacitance at different scan rates, charge-discharge curves, specific capacitance at different discharge current of WS_2 and RGO, comparison of energy density with specific capacitance. This material is available free of charge via the Internet at http://pubs.acs.org.

■ AUTHOR INFORMATION

Corresponding Author

*E-mail: csrout@iitbbs.ac.in.

Notes

The authors declare no competing financial interest.

■ ACKNOWLEDGMENTS

C.S.R. thanks the Department of Science and Technology, India, for the Ramanujan fellowship.

■ REFERENCES

(1) Geim, A. K. *Science* **2009**, *324*, 1530−1534.
(2) Novoselov, K. S.; Geim, A. K.; Morozov, S. V.; Jiang, D.; Zhang, Y.; Dubonos, S. V.; Grigorieva, I. V.; Firsov, A. A. *Science* **2004**, *306*, 666−669.
(3) Rao, C. N. R.; Sood, A. K.; Subrahmanyam, K. S.; Govindaraj, A. *Angew. Chem., Int. Ed.* **2009**, *48*, 7752−7777.
(4) Radisavljevic, B.; Radenovic, A.; Brivio, J.; Giacometti, V.; Kis, A. *Nature Nanotechnol.* **2011**, *6*, 147−150.
(5) Matte, H. S. S. R.; Gomathi, A.; Manna, A. K.; Late, D. J.; Datta, R.; Pati, S. K.; Rao, C. N. R. *Angew. Chem., Int. Ed.* **2010**, *122*, 4153−4156.
(6) Ross, J. S.; Wu, S.; Yu, H.; Ghimire, N. J.; Jones, A. M.; Aivazian, G.; Yan, J.; Mandrus, D. G.; Xiao, D.; Yao, W.; Xu, X. *Nat. Commun.* **2013**, *4*, 1474−1476.
(7) Larentis, S.; Fallahazad, B.; Tutuc, E. *Appl. Phys. Lett.* **2013**, *101* (223104), 1−4.
(8) Kong, D.; Wang, H.; Cha, J. J.; Pasta, M.; Koski, K. J.; Yao, Y.; Cui, Y. *Nano Lett.* **2013**, *13*, 1341−1347.
(9) Fang, H.; Chuang, S.; Chang, T. C.; Takei, K.; Takahashi, T.; Javey, A. *Nano Lett.* **2012**, *12*, 3788−3792.
(10) Jeong, S.; Yoo, D.; Jang, J. T.; Kim, M.; Cheon, J. *J. Am. Chem. Soc.* **2012**, *134*, 18233−18236.
(11) Xu, K.; Chen, P.; Li, X.; Wu, C.; Guo, Y.; Zhao, J.; Wu, X.; Xie, Y. *Angew. Chem., Int. Ed.* **2013**, *52*, 10477−10481.
(12) Kreis, C.; Werth, S.; Adelung, R.; Kipp, L.; Skibowski, M. *Phys. Rev. B* **2003**, *68* (235331), 1−6.
(13) Liu, C.; Frindt, R. F. *Phys. Rev. B* **1985**, *31*, 4086−4088.
(14) Ayari, A.; Cobas, E.; Fuhrer, O. *J. Appl. Phys.* **2007**, *101* (014507), 1−5.
(15) Brown, B. E. *Acta Crystallogr.* **1966**, *20*, 264−267.
(16) Castellanos-Gomez, A.; Navarro-Moratalla, E.; Mokry, G.; Quereda, J.; Pinilla-Cienfuegos, E.; Agraït, N.; van der Zant, H. S. J.; Coronado, E.; Steele, G. A.; Rubio-Bollinger, G. *Nano Res.* **2013**, *6*, 191−199.
(17) Galvis, J.A.; Rodiere, P.; Guillamon, I.; Osorio, M. R.; Rodrigo, J. G.; Cario, L.; Navarro-Moratalla, E.; Coronado, E.; Vieira, S.; Suderow, H. *Phys. Rev. B* **2013**, *87* (094502), 1−9.
(18) Zhu, Y.; Murali, S.; Stoller, M. D.; Ganesh, K. J.; Cai, W.; Ferreira, P. J.; Pirkle, A.; Wallace, R. M.; Cychosz, K. A.; Thommes, M.; Su, D.; Stach, E. A.; Ruoff, R. S. *Science* **2011**, *332*, 1537−1541.
(19) El-Kady, M. F.; Strong, V.; Dubin, S.; Kaner, R. B. *Science* **2012**, *335*, 1326−1330.
(20) Simon, P.; Gogotsi, Y. *Nat. Mater.* **2008**, *7*, 845−854.
(21) Hao, L.; Li, X.; Zhi, L. *Adv. Mater.* **2013**, *25*, 3899−3904.
(22) Naoi, A.; Naoi, W.; Aoyagi, S.; Miyamoto, J.-I.; Kamino, T. *Acc. Chem. Res.* **2013**, *46*, 1075−1083.
(23) Sumboja, A.; Foo, C.Y.; Wang, X.; Lee, P.S. *Adv. Mater.* **2013**, *25*, 2809−2815.
(24) Gopalakrishnan, K.; Moses, K.; Govindaraj, A.; Rao, C. N. R. *Solid State Commun.*. **2013**, http://dx.doi.org/10.1016/j.ssc.2013.02.005.
(25) Gopalakrishnan, K.; Govindaraj, A.; Rao, C. N. R. 2013, *1*, 7563-7565.
(26) Sreedhara, M. B.; Ramakrishna Matte, H. S. S.; Govindaraj, A.; Rao, C. N. R. *Chem. An Asian J.* DOI: 10.1002/asia.201300470.
(27) Dong, X.-C.; Xu, H.; Wang, X. W.; Huang, Y.-X.; Chan-Park, M. B.; Zhang, H.; Wang, L.-H.; Huang, W.; Chen, P. *ACS Nano* **2012**, *6*, 3206−3213.
(28) G. Zhang, G.; Lou, X.W. *Adv. Mater.* **2013**, *25*, 976−979.
(29) Jo, C.; Hwang, J.; Song, H.; Dao, A. H.; Kim, Y.-T.; Lee, S. H.; Hong, S. W.; Yoon, S.; Lee, J. *Adv. Funct. Mater.* **2013**, *23*, 3747−3754.
(30) Mai, L.; Li, H.; Zhao, Y.; Xu, L.; Xu, X.; Luo, Y.; Zhang, Z.; Ke, W.; Niu, C.; Zhang, Q. *Sci. Reports* **2013**, *3* (1718), 1−8.
(31) Shiva, K.; Rajendra, H. B.; Subrahmanyam, K. S.; Bhatacharyya, A. J.; Rao, C. N. R. *Chem.—Eur. J.* **2012**, *18*, 4489−4494.
(32) Feng, J.; Sun, X.; Wu, C.; Peng, L.; Lin, C.; Hu, S.; Yang, J.; Xie, Y. *J. Am. Chem. Soc.* **2011**, *133*, 17832−17838.
(33) Cao, L.; Yang, S.; Gao, W.; Liu, Z.; Gong, Y.; Ma, L.; Shi, G.; Lei, S.; Zhang, Y.; Zhang, S.; Vajtai, R.; Ajayan, P. M. *Small* **2013**, *9*, 2905−2910.
(34) Zhang, L.; Wu, H. B.; Lou, X. W. *Chem. Commun.* **2012**, *48*, 6912−6914.
(35) Wang, Q.; Jiao, L.; Du, H.; Yang, J.; Huan, Q.; Peng, W.; Si, Y.; Wang, Y.; Yuan, H. *Cryst. Eng. Comm.* **2011**, *13*, 6960−6963.
(36) Wang, B.; Park, J.; Su, D.; Wang, C.; Ahnb, H.; Wang, G. *J. Mater. Chem.* **2012**, *22*, 15750−15756.
(37) Zhu, T.; Wang, Z.; Ding, S.; Chen, J. S.; Lou, X. W. *RSC Adv.* **2011**, *1*, 397.
(38) Yang, J.; Duan, X.; Qin, Q.; Zheng, W. *J. Mater. Chem. A* **2013**, *1*, 7880−7884.
(39) Mate, H. S. S. R.; Maitra, U.; Kumar, P.; Rao, B. G.; Pramoda, K.; Rao, C. N. R. *Z. Anorg. Allg. Chem.* **2012**, *638*, 2617−2624.
(40) Georgiou, T.; Jalil, R.; Belle, B. D.; Britnell, L.; Gorbachev, R. V.; Morozov, S. V.; Kim, Y.-J.; Gholinia, A.; Haigh, S. J.; Makarovsky, O.; Eaves, L.; Ponomarenko, L. A.; Geim, A. K.; Novoselov, K.S.; Mishchenko, A. *Nat. Nanotechnol.* **2013**, *8*, 100−103.
(41) Braga, D.; Lezama, I.G.; Berger, H.; Morpurgo, A. F. *Nano Lett.* **2012**, *12*, 5218−5223.

(42) Fang, X.; Hua, C.; Wu, C.; Wang, X.; Shen, L.; Kong, Q.; Wang, J.; Hu, Y.; Wang, Z.; Chen, L. *Chem.—Eur. J.* **2013**, *19*, 5694−5700.
(43) Liu, H.; Su, D.; Wang, G.; Qiao, S. Z. *J. Mater. Chem.* **2012**, *22*, 17437−17440.
(44) Bhandavat, R.; David, L.; Singh, G. *J. Phys. Chem. Lett.* **2012**, *3*, 1523−1530.
(45) Wua, Z.; Fang, B.; Bonakdarpour, A.; Suna, A.; Wilkinsonb, D. P.; Wanga, D. *Appl. Catal. B* **2012**, *125*, 59−66.
(46) Alonso, G.; Petranovskii, V.; Del Valle, M.; Cruz-Reyes, J.; Licea-Claverie, A.; Fuentes, S. *Appl. Catal. A* **2000**, *197*, 87−97.
(47) Tenne, R.; Margulis, L.; Genut, M.; Hodes, G. *Nature* **1992**, *360*, 444−446.
(48) Rout, C.S.; Kim, B.H.; Xu, X.; Cho, J.P.; Shin, H.S. *J. Am. Chem. Soc.* **2013**, *135*, 8720−8725.
(49) M. Virsek, M.; A. Jesih, A.; I. Milosevic, I.; M. Damnjanovic, M.; M. Remskar, M. *Surf. Sci.* **2007**, *601*, 2868−2872.
(50) Berkdemir, A.; Gutiérrez, H.R.; Botello-Méndez, A.R.; Perea-López, N.; Laura Elías, A.; Chia, C.; Wang, B.; Crespi, V.H.; López-Urías, F.; Charlier, J.; Terrones, H.; Terrones, M. *Sci. Reports* **2013**, *3* (1755), 1−8.
(51) Hu, L.; Chen, W.; Xie, X.; Liu, N.; Yang, Y.; Wu, H.; Yao, Y.; Pasta, M.; Alshareef, H. N.; Cui, Y. *ACS Nano* **2013**, *5*, 8904−8913.
(52) Tao, J.; Liu, N.; Ma, W.; Ding, L.; Li, L.; Su, J.; Gao, Y. *Sci. Reports* **2013**, *3* (2286), 1−7.
(53) Huang, K.-J.; Wang, L.; Liu, Y.-J.; Liu, Y.-M.; Wang, H.-B.; Gan, T.; Wang, L.-L. *Int. J. Hydrogen Energy* **2013**, http://dx.doi.org/10.1016/j.ijhydene.2013.08.112.
(54) Hu, B.; Qin, X.; Asiri, A.M.; Alamry, K.A.; Al-Youbi, A.O.; Sun, X. *Electrochem. Commun.* **2013**, *28*, 75−78.